

The structure of spiral galaxies - I. Near-infrared properties of bulges, disks and bars

M.S. Seigar & P.A. James

*Astrophysics Group, Liverpool John Moores University, Byrom St., Liverpool, L3 3AF, U.K.
email: mss & paj @staru1.livjm.ac.uk*

23 August 2018

ABSTRACT

We present data for a sample of 45 spiral galaxies over a range of Hubble types, imaged in the near-IR J and K bands. Parameters are calculated describing the bulge, disk and bar K-band light distributions, and we look for correlations showing the interrelation between these components.

We find that bulge profiles are not well-fitted by the classic de Vaucouleurs profile, and that exponential or $R^{1/2}$ fits are preferred. Bulge-to-disk ratio correlates only weakly with Hubble type. Many of the galaxies show central reddening of their J–K colours, which we interpret as due to nuclear starbursts or dusty AGN.

We define a new method for measuring the strength of bars, which we call Equivalent Angle. We stress that this is better than the traditional bar-interbar contrast, as it is not subject to seeing and resolution effects.

Bars are found in 40 of the 45 galaxies, 9 of which had been previously classified as unbarred. Bar strengths are found not to correlate with disk surface brightness or the presence of near neighbours, but a tendency is found for the most strongly barred galaxies to lie within a restricted, intermediate range of bulge-to-disk ratio. Bar light profiles are found to be either flat or exponentially decreasing along their long axes, with profile type not correlating strongly with Hubble type. Bar short axis profiles are significantly asymmetric, with the steeper profile being generally on the leading edge, assuming trailing arms. In the K-band we find bars with higher axial ratios than have been found previously in optical studies.

Key words: galaxies: spiral–galaxies: structure–galaxies: fundamental parameters

1 INTRODUCTION

This paper is the first in a study of the structure of spiral galaxies, in which we aim to look at the interrelation between bulges, disks, bars and spiral arms of galaxies over a wide range of Hubble types. We will attempt to constrain or distinguish between the various theories of formation and evolution of bar and spiral structures, and our results should also provide useful determinations of galaxy parameters for input into simulations of the evolution of galactic structures. The most controversial question in this area still concerns the origin of the spiral structure seen in most gas-rich disk galaxies, which is variously claimed to be due to quasi-stationary density wave modes (Lin & Shu 1964, 1966; Bertin et al. 1989a,b), stochastic self-propagating star formation (Gerola & Seiden 1978) or driving by nearby neighbours or central bars (Kormendy & Norman 1979), and we will discuss this in a future paper (Seigar & James 1997; paper II). However, there are also unresolved questions con-

cerning the origin of bars, and of the Hubble sequence of galaxy types, which we address in the present paper.

Our main technique is to image a large sample of galaxies in the near-IR J and K bands (centred on 1.3 and 2.2 μ m respectively), which has become generally accepted as the most powerful technique for revealing the structure of the dominant stellar mass component in galaxies. The advantages of this wavelength range are the relative freedom from extinction effects compared with visual imaging, and that the near-IR light from normal galaxies arises from the old stellar population which dominates the stellar mass. Whilst this latter claim has sometimes been contested on the grounds that luminous giants and supergiants could in principle dominate the near-IR light of a galaxy with recent star formation, Rix & Rieke (1993) indicate that the supergiant contribution to the K-band light from normal galaxies is at most 15–25%, a small effect compared to the impact of extinction and star formation on the visual morphology of star-forming galaxies.

Quantitative measurements will be presented for all of the stellar components of the galaxies (disks, bulges, bars and arms) to enable us to study the interrelations between them. This will provide the perfect database for a test of secular models of galaxy evolution (Combes et al. 1990; Courteau, de Jong & Broeils 1996) where bar-induced star-formation and mass transfer provide the central mechanism for the transformation of disk galaxies along the Hubble sequence. Another aim of this study is to produce realistic parameters which can be used both as input parameters for models of disk galaxies, and to compare with the output from such models.

This paper will describe the acquisition and reduction of the near-IR imaging data, and the analysis of the properties of the disks, bulges and bars of the full sample of 45 galaxies. The interrelation between the properties of these components will be investigated in detail, but spiral arm structure will be dealt with in a future paper (Seigar & James 1997, paper II). Section 2 describes the sample selection and observations; section 3 describes data reduction techniques; section 4 describes properties of bulges; section 5 describes properties of disks; section 6 describes properties of bars and section 7 contains a discussion and conclusions.

2 OBSERVATIONS

Observations are presented for a sample of 45 spiral galaxies, selected using the NASA/IPAC Extragalactic Database* (henceforth NED) on the basis of their diameters (<1.5 arcmin at the B_{25} isophote) and their face-on orientations (axial ratio $(b/a) > 0.5$, typically 0.8). They were specifically selected to span the full range of Hubble types Sa–Sd, on the basis of their classification in the Third Reference Catalog of Bright Galaxies (de Vaucouleurs et al. 1991; henceforth RC3), and no attempt was made to select a statistically representative or complete sample. A Hubble constant of 50 $\text{km s}^{-1} \text{Mpc}^{-1}$ is assumed throughout.

The data were obtained with the 3.8 metre United Kingdom Infrared Telescope (UKIRT) on Mauna Kea, using the near-IR camera IRCAM3. The observing dates were 1995 February 4–6 and 1995 November 17–19, with further images being taken on the nights 1996 May 21 and 22 as a backup for a programme which could not be carried out through the prevailing thin cirrus. Conditions were generally photometric for the first two runs, and the seeing was typically sub–arcsecond. However, the stability and guiding of UKIRT at that time were such that images were sometimes enlarged at the 1 arcsec level by telescope motions, particularly in the RA direction. This can have the effect of smearing the point spread function (PSF), but as it is of the order of the seeing, its effect is small in these observations. IRCAM3 is a 256×256 InSb array camera, with a pixel scale of 0.286 arcsec, giving an image scale of 73×73 arcsec. The galaxies were imaged in the standard J ($1.3 \mu\text{m}$) and K ($2.2 \mu\text{m}$) filters. Typical total exposures were 9 and 30 minutes

* The NASA/IPAC Extragalactic Database (NED) is operated by the Jet Propulsion Laboratory, California Institute of Technology, under contract with the National Aeronautics and Space Administration.

per galaxy at J and K respectively, with each exposure being split into several jittered sub-exposures to facilitate bad pixel removal. These observations result in a detection of 20.5 magnitudes per square arcsec at 1σ per pixel at K and 21.5 magnitudes per square arcsec at J. Equal times were spent observing nearby blank sky in the same jitter pattern to produce a median sky flat for each galaxy. Near-IR standard stars from the UKIRT faint standards list were observed throughout the photometric nights for calibration purposes. Photometric errors are calculated to be at the 3% level. Photometry was also checked against previous work. Only one galaxy (NGC 6574) had been previously observed in these wavebands before and this had been using aperture photometry and has been reported by Balzano & Weedman (1981). They report values within a 10.1 arcsec aperture of a K-band magnitude of 10.14 ± 0.10 and a J-band magnitude of 11.28 ± 0.05 . Within the same aperture we get a magnitude of 10.13 ± 0.04 at K and a magnitude of 11.24 ± 0.16 at J.

3 DATA REDUCTION

Initial data reduction was entirely standard and will therefore be described only briefly. The STARLINK packages KAPPA and FIGARO were used for basic image processing. All frames were dark-subtracted, with bias subtraction not being needed due to the non-destructive read mode of operation of IRCAM3. Sky flats were constructed by taking medians of sky frames taken within ~ 30 minutes of the given galaxy observations, since experimentation showed that variations in either the array or in the sky colour gave increased noise if more sky frames were included in the median. The individual galaxy integrations were then flat-fielded, and all known bad pixels set to magic values such that they were ignored when the images were added to give the final mosaics. The individual images were sky-subtracted prior to this final addition, by taking a mean of the median brightnesses over a 25×25 pixel box in each of the four corners of all of the frames. The images of the standards were similarly dark-subtracted, flat-fielded and had their bad pixels removed, prior to photometry being measured using 12 arcsec software apertures.

The RGASP package was then used to fit ellipses to the isophotes in the reduced galaxy images. The ellipticity of the outermost ellipses was then adopted and the PROF routine, which takes medians around ellipses at increasing radii, was run keeping this ellipticity and position angle constant. The REBUILD facility in RGASP enables a simulated galaxy to be made up using the ellipticity and position angle and the median surface brightness calculated around these ellipses, and subtracting this rebuilt image from the original image removes the elliptically-symmetric bulge and disk components. This procedure leaves an image of the bar and spiral arms. Plotting the surface brightness of the fitted ellipses as a function of semi-major axis gives the light profiles shown in figure 1, which will be used to do a one-dimensional bulge–disk decomposition below.

The bulge– and disk–subtracted galaxy images were then deprojected in an attempt to overcome inclination effects on the spiral arm pattern and bar morphology, using a similar technique to that of Elmegreen & Elmegreen (1984).

This was done by measuring the disk major and minor axes at an isophote well out in the disk, where any ellipticity is plausibly due to inclination effects (although Rix & Zaritsky (1995) have demonstrated that there is measurable ellipticity even in face-on spiral galaxies, which introduces some uncertainties into this process). The images were then rotated to make the measured major axis vertical, and the minor axis was then stretched by a factor equal to the measured major/minor axis ratio. This correction was always quite small, given the generally face-on nature of galaxies in this sample.

4 PROPERTIES OF BULGES

Bulge-to-disk ratio (B/D) has always been taken as a key parameter in defining the position of a galaxy on the Hubble sequence. This ratio can be significantly affected by extinction in the visual, and K-band imaging clearly gives a much more reliable indication of the stellar mass in the disks and bulges of spiral galaxies. B/D was calculated for all the galaxies in the present sample, using a one-dimensional profile deconvolution technique on the K-band light profiles (figure 1). De Jong (1996a) has demonstrated that there are some advantages in doing a full two-dimensional fit to the galaxy images when determining disk and bulge profiles, but the advantages are not huge and outweighed, for the present study, by the greatly increased complexity of the fitting process.

In order to separate the bulge and disk components of a measured light profile, some assumptions have to be made about the functional form of the individual components, and the reliability of the results necessarily depends on how good an approximation these forms are to the true light distributions (see Capaccioli & Caon 1992 for a general discussion of profile decomposition techniques). Traditionally disks have been represented by an exponential light distribution and bulges by the $R^{1/4}$ light distribution found by de Vaucouleurs (1953) to be an excellent fit to the light profiles of most elliptical galaxies. Recently, however, Andredakis & Sanders (1994) and de Jong (1996b) have demonstrated that most bulges, particularly those of late-type spirals, are better represented by exponentials, with a scale length about an order of magnitude smaller than that of their disks. This follows earlier suggestions that NGC 4565 (Frankston & Schild 1976) and the Milky Way (Kent, Dame & Fazio 1991) have exponential bulges. Even the bulges of early-type galaxies were found by de Jong (1996b) to be better fitted by either exponentials or $R^{1/2}$ profiles, where the latter are intermediate between the exponential form and the much cuspier de Vaucouleurs profile. For our study we elected to leave the index in the fitted bulge light profile as a free parameter, which had the dual advantage of allowing the best fit to the bulge profile to be found, and of enabling us to investigate any possible change in the best-fit bulge index with B/D ratio, as indicated by de Jong (1996b). The fit was performed using a Levenberg-Marquardt method which reduces the value of χ^2 of a fit of the analytical profile to the measured surface brightness, μ , as a function of radius, r . The method fits to data and outputs the bulge half-light radius and surface brightness at that radius, disk central surface brightness, disk scale length, disk central surface brightness

and bulge-profile index for which it finds the lowest value for χ^2 .

An important issue in galaxy profile fitting is atmospheric seeing, which is particularly likely to affect the measured bulge parameters by smoothing out the light from the central, fairly cuspy region. We quantified the effects of seeing on measured parameters by constructing artificial galaxies with profiles typical of the galaxies in our sample, smoothing by a Gaussian to simulate seeing effects, and then adding noise. These artificial galaxies were then analysed using the same data reduction process as for the real images, to assess how well the software can extract the profile parameters, both with and without the effects of seeing. The results are given for two of these simulated galaxies in Table 1, where the values given are the input and recovered values of bulge surface brightness, half-light radius and power law, disk central surface brightness and disk scale length, with simulated seeing of 0.85 arcsec, typical of the real images. (With no simulated seeing, all parameters were recovered without error.) Simulated galaxy (a) has bulge parameters typical of the galaxy sample, whereas (b) represents a worst case, with a low-luminosity, short scale-length bulge ($B/D \sim 0.08$). Table 1 shows that the effects of seeing are small, affecting measured parameters by at most 10%, which is likely to be within the random errors. Effects on disk parameters were found to be of a similar order. Thus no specific seeing corrections were applied to these images, or to any parameters derived from them. This technique also allowed us to estimate errors for the fitted parameters. However, where the disk starts to get down to the sky level, errors in determining the sky level have been assumed to be the dominant source of error in determining the disk parameters. As a result of these systematic effects we believe that the typical error associated with our measurement of the bulge-profile index is about ± 0.05 .

The measured parameters of the bulges are shown in table 2. These have been converted into physical quantities using distances calculated assuming a constant Hubble flow. Note that the profile fit of the galaxy ESO 555 -G 013 revealed that this was almost completely dominated by disk and as a result the fit could not produce a stable fit to the bulge. We could therefore not constrain the bulge parameters for ESO 555 -G 013 and thus a bulge-to-disk ratio was not calculated.

Looking at the derived properties of the bulges, we first confirm the conclusion of de Jong (1996b) that better bulge fits are given by a bulge-profile index between 1/2 and 1 (the two values adopted by de Jong) than with the de Vaucouleurs $R^{1/4}$ profile. Indeed, there is some evidence for a bimodal distribution, with indices around these two values being preferred. However, no strong correlation was found (correlation coefficient=0.33; significance=97%) between this index and Hubble type (figure 2), whereas de Jong found that values less than 1 tended to be found only in early-type galaxies. This distribution is in good agreement with that found by Andredakis, Peletier & Balcells (1995) over the same range in Hubble type. There is also no significant correlation between best-fit bulge index and bulge luminosity (correlation coefficient=0.17; significance=76% - see figure 3), which differs from the case for dwarf elliptical galaxies, where smaller power-law indices and cuspier profiles tend to

be found in the more luminous galaxies (Young & Currie 1994; James 1994).

4.1 AGN or starburst contributions to bulge light

A final concern with the bulge profiles is that they may be contaminated by emission from active galactic nuclei (AGN). It is hard to constrain such a component simply from the light profile, since even quite a prominent point source can be indistinguishable from a cuspy bulge light distribution. However, colours do provide a useful diagnostic, since AGN are generally heavily extinguished, giving much redder near-IR colours than the surrounding stellar bulge (Glass & Moorwood 1985). We thus combined central J and K light profiles to give radial colour maps for all galaxies, which we could use to search for any trend towards red J–K colours in the very central regions. The seeing for each frame in each band was calculated using the PSF routine in the STARLINK KAPPA package. It was typically found to be approximately the same in both the J- and K-bands, at ~ 0.8 arcsec. The typical photometric errors in the central colour changes are therefore calculated to be at the 1% level.

Representative J–K profiles are shown in figure 4. Disk colours generally lie between J–K of 0.7 and 1.0, consistent with the expectations for a fairly blue, star-forming system. Approximately 50% of our galaxies show no central colour change whatever at the 0.1 mag level (e.g. UGC 3296 in Figure 4). Of the remainder, the nuclear colour changes vary between a just-detectable increase of ~ 0.1 mag to over a magnitude, with the reddest nuclear colours approaching J–K=2.0 (UGC 3707 and IC 568, shown in figure 4). We never see a nucleus bluer than the surrounding disk.

J–K values between 1.0 and 2.0 could be the result of either a dusty starburst, or of a dust-embedded AGN. Glass & Moorwood (1985) show that JHKL colours have some power in distinguishing between these possibilities, but we do not have the required observations to apply this to our galaxies. However, there does appear to be useful information in the radial profile of the nuclear colour change. Comparing the colour profiles of IC 568 and UGC 3707, it is clear that the redward trend starts much further out for IC 568, whereas the red nucleus of UGC 3707 is very small, and almost certainly unresolved. Thus we claim that the latter galaxy probably hosts an AGN, and the former an extended starburst nucleus. Supporting evidence for a nuclear starburst in IC 568 comes from its having a very strong bar, a feature often linked with enhanced central star formation (e.g. Roberts, Huntley & van Albada 1979; Huang et al. 1996). (However, it should also be noted that UGC 3707 has a very strong bar.) We also show in Paper II that IC 568 has the second largest far-IR luminosity of any of the galaxies studied here, which is almost certainly linked to its nuclear activity.

Of the galaxies showing clear nuclear reddening ($\Delta(J-K) > 0.2$), 7 show evidence for an extended red component (UGC 357, NGC 2503, IC 742, IC 1809, IC 1196, UGC 3806 and IC 568, in order of increasing strength), and 3 have unresolved red nuclei (UGC 850, UGC 3839 and UGC 3707)

5 PROPERTIES OF DISKS

The bulge/disk deconvolution described in the previous section also yielded parameters for the best-fitting exponential to the disks of all galaxies in the sample. Given that we chose to use only exponentials, there are only two parameters in the disk fit for each galaxy, the central surface brightness and the scale-length in kpc of the best-fitting exponential. These are tabulated in columns 2 and 3 of Table 3, which summarises the disk and bar parameters for the 45 spiral galaxies. Columns 4 and 5 give the disk K-band absolute magnitude and K-band bulge-to-disk ratio respectively.

The disk central surface brightnesses have been corrected using the following equation given by de Jong (1996),

$$\mu^i = \mu - 2.5C \log \left(\frac{a}{b} \right) \quad (1)$$

where μ^i is the corrected surface brightness, μ is the measured surface brightness, a is the major axis, b is the minor axis and C is a factor dependent on whether the galaxy is optically thick or thin. If $C = 1$ then the galaxy is optically thin, if $C = 0$ then the galaxy is optically thick. De Jong (1996b) uses the optically thin case and we adopt this approach.

The distribution of disk central surface brightnesses has been analysed many times since the classic study by Freeman (1970), who discovered a very narrow measured range in this parameter, since termed the Freeman Law. This has recently been comprehensively reanalysed by de Jong (1996b), who used near-IR photometry to minimise possible extinction effects. Whilst de Jong confirmed that there is a sharp cutoff in the high surface brightness side of the distribution, he found that after accounting for selection effects, there was no such cutoff on the low surface brightness side. Thus the overall distribution in disk surface brightness is much broader than claimed by Freeman (1970).

The present sample of galaxies was not selected as an unbiased statistical sample for the type of study undertaken by de Jong (1996b). However, it is still instructive to compare the distribution of disk parameters with those found by de Jong, prior to his application of the selection effect corrections. Figure 5 shows disk central surface brightnesses plotted against total disk luminosity, which can be compared with the distributions in both parameters found by de Jong. We find a range of disk K absolute magnitudes predominantly lying between –22 and –26, with two fainter disks at $M_K \sim -21$. De Jong (1996b) finds exactly the same range and distribution in disk luminosity, once the different assumed Hubble constants are taken into account. The agreement for disk central surface brightnesses in the K-band is somewhat less good, however. We find a range of just over 3 mag. in this parameter, 16.1–19.5 mag., and also find absolutely no correlation with Hubble type (figure 6). Comparing this distribution with figure 3 of de Jong (1996b), he finds a wider range, extending to both higher and lower surface brightnesses. Almost all of his very low surface brightness disks are extreme late-type galaxies which we do not have in our sample, but the excess of high-surface-brightness disks, at ~ 16 K mag./arcsec², is harder to understand. All of these galaxies in de Jong's sample lie between Hubble types Sb–Sc, and figure 6 shows that we detect no such galaxies. However, on the whole there is no evidence for any systematic offsets

in photometry between our data and de Jong (1996b), and any differences are probably due to sample selection.

In Hubble's classification scheme, the position of a galaxy along the sequence was thought to be determined largely by the relative dominance of the bulge and disk. However, figure 7 shows that this correlation is fairly weak when near-IR parameters are used. This figure shows the fraction of the total K- band luminosity of the galaxy which is represented by the disk, plotted as a function of catalogued Hubble type from RC3. In general, the later type galaxies do appear somewhat more disk-dominated, as Hubble's scheme would predict, but there is a large scatter in this correlation, and again we confirm a conclusion of de Jong (1996b), in that B/D ratio is not in fact the central parameter in determining Hubble type. De Jong (1996b) concludes that spiral arm type must instead be the main determinant of morphological type, a suggestion which we will discuss in Paper II.

In figure 8 we show that there is a weak correlation between disk scale lengths and bulge half-light radii (correlation coefficient 0.50, significance 99.83%) with a mean ratio of 5.4. This is a very similar result to that found by Courteau et al. (1996), although they chose to plot the measured scale-lengths in arcsec to avoid bias by resolution effects. We feel that biases caused by the spread of distances to our galaxies will be more significant in potentially causing spurious correlations, so we prefer to plot absolute scalelengths. Another difference is that Courteau et al. fitted bulges by exponentials only, whereas we leave bulge index as a free parameter, but again this change does not destroy the correlation. Courteau et al. (1996) interpret the correlation as evidence for secular models, where bulges are assembled gradually through a series of bar instabilities, as this theory directly links properties of disks and bulges. It is also interesting to note that Aaronson, Huchra & Mould (1979), in one of the first attempts to find a physical basis for the Tully-Fisher relation (Tully & Fisher 1977) between luminosity and rotational velocity in spiral galaxies, found it necessary to invoke a universal mass profile for spirals, which is not a strong function of Hubble type. Figures 7 and 8 may provide some evidence for this universal profile in the K-band light distributions.

Figure 9 shows the distribution of disk central surface brightness as a function of disk exponential scale length, which shows a reasonably significant correlation (correlation coefficient 0.56, significance 99.97%). Again, this is very similar to the distribution given in de Jong (1996b), once differences in assumed Hubble constant are accounted for. We confirm the lack of high-surface brightness, long-scale-length disks, which cannot be the result of selection effects, whereas the cut-off at low surface brightness certainly is due to selection.

6 PROPERTIES OF BARS

We now consider the properties of the bar components as revealed by our imaging, again focussing principally on the K band images to minimise the effects of dust obscuration. For simplicity, we adopt as a working definition of a bar, that part of the central light distribution which is left when the elliptically-symmetric disk and bulge components have been

subtracted (in this case, using the RGASP REBUILD facility). Thus we include in this definition all oval distortions of the bulge and central disk as discussed by various authors. Also, there is potential confusion between the outer bar and the inner parts of the spiral arms or other disk asymmetries, which are also left after the REBUILD subtraction. In general, there is a sharp bend or a discontinuity between the end of the bar and the beginning of the arms which averts this problem, but there are some cases (e.g. IC 357) with S-shaped bar/arm morphologies, where the arms sweep back gradually from the ends of the bar, and the definition of the bar end is somewhat arbitrary.

The first and very striking result is how common bars are revealed to be in this galaxy sample. Of the 45 galaxies studied, 31 are classified as barred on the basis of their optical morphologies in RC3, a similar barred fraction to previous optical studies. However, a visual analysis of the K-band images reveals evidence for bars in a further 9, giving a final barred fraction of about 90%. Our initial selection was not biased towards barred galaxies, so this fraction should be representative of the general population of bright spiral galaxies. We note that the combination of near-IR imaging and the subtraction of the disk and bulge makes this study particularly sensitive to the detection of weak bars, which accounts for the higher barred fraction than any previous study of which we are aware, although there has been a trend for estimates of the barred fraction to increase with time. De Vaucouleurs (1963) claimed that just one-third of disk galaxies have bars, whereas more recent estimates generally put the figure at about two-thirds. Given our present findings, it is tempting to speculate that bars may always be present in disk galaxies at some level.

We now attempt to quantify the strength of the bars detected in these galaxies. Since there is no generally accepted method for doing this, and since it is central to our analysis, we have defined our own procedure for producing repeatable and objective measures of the bar strength. In Paper II we will apply essentially the same method to determining arm strengths in the same galaxies. The key problem is to find a measure which is not systematically affected by the quality of the observational material used, and in particular by the noise level and seeing effects. This means that, for example, the traditional method of taking the peak intensity at the centre of the bar and ratioing this by the disk intensity at the same radial distance to produce a bar-interbar contrast is not satisfactory, since poor seeing conditions will smooth out the bar emission and decrease this contrast. The most robust measure we can think of is closely analogous to the quantity Equivalent Width which is widely used in spectroscopy, and is specifically designed to be independent of noise and resolution effects. We term our analogous quantity Equivalent Angle, henceforth EA, and define it to be the angle subtended at the center of the galaxy by a sector of the underlying disk and bulge which emits as much light as does the bar component, within the same radial limits (see figure 10 for a diagrammatic representation of EA). Thus a bar which emitted as much light as the underlying disk between, say, 0.5 and 1.0 kpc radius would have an EA of 180° (not 360° since we define EA to refer to one end of the bar, and the other end in this case would also contribute 180°) within these radial limits. We derive EA as a function of radius, but also take a mean value over the whole detected

radial extent of the bar to parametrise the strength of the bar as a whole, normalised to the surface brightness of the underlying galaxy. The errors in EA are derived from errors in the calculated position angle (PA), ellipticity and sky levels. The errors in PA and ellipticity are important because EA is always calculated in a polar coordinate frame ($\ln R, \theta$). Both the difference and rebuild images are converted to polar coordinates. The rebuild image in the polar coordinate frame should not have variations in surface brightness with azimuthal angle, but errors in the PA and ellipticity can introduce variations in this.

Overall bar strengths, bar lengths and bar widths are tabulated in table 3. Figure 11 shows a histogram of the overall EA values for the 40 galaxies with detected bars, with the shaded areas representing bar strengths for those galaxies with nearby neighbours. Neighbours are defined, somewhat arbitrarily, as galaxies of comparable luminosity to the observed galaxy, at a projected distance within 6 diameters of the observed galaxy. In general redshifts are not available and so chance line-of-sight associations cannot be excluded. Probably unsurprisingly, no strong dependence of bar properties on the presence of such neighbours is found, supporting the conventional view that bars are intrinsic features of disk galaxies, and occur as a result of disk instabilities. The overall bar strengths can be compared with the values quoted by Ohta, Hamabe & Wakamatsu (1990), who find that bars comprise between 24% and 47% of the total galaxy light within the radii occupied by the bars. These convert to EA of $\sim 40^\circ$ – 85° , which is consistent with the range of values we find for strongly barred galaxies (Ohta et al. 1990) specifically selected galaxies with strong bars).

It is then of interest to test whether there are any observable properties of disks which make them particularly susceptible to the formation of bars. Theoretical analysis and simulations suggest that bar instabilities arise as a natural consequence of cold, self-gravitating disks, and that the bar mode can only be suppressed by the presence of a dynamically warm stabilising component, such as a massive bulge or spheroidal halo (Hohl 1971; Ostriker & Peebles 1973). We can test such effects by correlating bar strength with the measured properties of the bulges and disks of our galaxies. Figure 12 shows bar strength plotted as a function of the disk central brightness, and we find no overall dependence in the expected sense. Indeed, if anything the strongest bars tend to be found in the lowest surface brightness disks, although this is not a significant correlation. Figure 13 shows that there is also no overall trend between bar strength and bulge- to-disk ratio, although there is evidence that the most strongly barred galaxies have B/D values falling in a very narrow range. The 10 most strongly barred galaxies all have B/D between 0.28 and 0.52, compared with a full range of B/D from 0.04 to 1.56. A statistical test showed that the spread in B/D values for the strongly barred ($EA > 30^\circ$) galaxies is narrower than that of the overall sample at the 99.92% ($> 3\sigma$) level. This is quite a striking result, and it is hard to see how it would come about as a result of systematic effects. Whilst the sample is in no sense statistically complete, the strength of the bar was not included in the selection criteria, which were purely defined in terms of Hubble type, diameter and inclination. Even if there were some selection systematic which correlated with classified Hubble type, we have shown that this latter cor-

relates only weakly with B/D. The correlation cannot be a simple effect of the type that bright bars live in bright galaxies because the definition of bar strength in terms of EA effectively normalises bar strength to the luminosity of the surrounding bulge and disk.

It is hard to find any theoretical explanation for strong bars preferentially inhabiting galaxies of intermediate B/D. It is still generally thought that the bar instability results from a cold disk whose kinematics are dominated by rotation (Ostriker & Peebles 1973). The much discussed secular theory of galaxy evolution (Combes et al. 1990; Pfenniger & Norman 1990) postulates that this instability may provide a mechanism for enhancing the bulge, since bars are known to funnel material from the disk into the central regions. Accretion of a large amount of mass in the centre ultimately destroys the bar (Friedli & Benz 1993), stopping or at least interrupting the evolutionary process, but overall this appears to be a viable mechanism for the evolution of isolated galaxies along the Hubble sequence. However, this does not lead to any obvious correlation between bar strength and B/D, except that one might see a generally declining bar strength with increasing dominance of the bulge. Indeed, if secular evolution is the dominant process in determining the Hubble sequence, then Figure 13 would imply that galaxies of intermediate B/D should be quite rare, as the strong bars would rapidly evolve galaxies through this state. Clearly this simplistic analysis does not fit the observed distribution of B/D values. Another similar plot (not shown) of bar EA against the ratio of the disk scale length to the bulge half-light radius (h/r_e) also revealed that the strongest bars fall in a narrow range of h/r_e from $\simeq 4.6$ to 6.2.

We now move on from a discussion of the overall strength of bars to the light distribution within individual bars. There has been relatively little previous work on this subject, and one of the few analytic distributions proposed for bar light is that of Freeman (1966):

$$\Sigma_{bar}(x, y) = \Sigma_{0,bar}(1 - (x/a_{bar})^2 - (y/b_{bar})^2)^{\frac{1}{2}}, \quad (2)$$

where $\Sigma_{0,bar}$ is the bar central surface brightness, and a_{bar} and b_{bar} are the semi-major and semi-minor axes respectively. This gives a profile that is flat in the central regions, then falling increasingly steeply to zero at $x = a_{bar}$ along the major axis and $y = b_{bar}$ along the minor axis. Beyond these limits it takes imaginary values, and must be set to zero. Observational studies of bar profiles (Elmegreen & Elmegreen 1985; Baumgart & Peterson 1986; Ohta et al. 1990; Elmegreen et al. 1996) find a range of profile types. All of these studies claim that at least some bars show exponential profiles along their major axes, and the N-body simulations of Miller & Smith (1979) provide some theoretical justification for the existence of such bar profiles. However, some galaxies are also found to have flat major axis profiles, which more nearly resemble the functional form proposed by Freeman (1966). Elmegreen et al. (1996) conclude that the flat bars tend to be stronger compared to the galaxy luminosity, and are found in earlier Hubble types, whereas the weaker exponential bars are found preferentially in late-type spirals.

We measured bar profiles in three ways, starting in two cases from the bulge- and disk-subtracted, inclination-corrected K-band images. From these we calculate both the bar EA (defined above) as a function of radius, which gives

a strength normalised to bulge and disk surface brightness, and also major and minor axis profiles obtained by summing flux in slices oriented perpendicular to the appropriate axis. Finally, we use the non-subtracted K-band images to look at major axis profiles, so as to compare them with the bar light-profiles of Elmegreen et al. (1996).

Considering these major and minor axis profiles first, we confirm some of the conclusions reached by Elmegreen et al. (1996). Figure 14 shows three representative K-band bar profiles in both the subtracted cases (right column) and non-subtracted cases (left column). The non-subtracted bar profiles illustrate that we find two main types of bar profiles. We find flat profiles (IC 357 and IC 568), which are characterised by a flat plateau, with a break at the end of the major axis and a steep descent at large radii, and weaker, exponentially decreasing bars (e.g. NGC 5737). Both types were also found by Elmegreen et al. (1996). Also plotted in figure 14 are bar major-axis profiles found for galaxies after subtraction of the ellipse-fit model (right column). In the case of IC 568, this is seen to rise at low radii, reach a plateau at intermediate radii, and then decrease at high radii. The bar in IC 568 is classified as flat and therefore it is not surprising that the bulge- and disk-subtracted bar profile reaches a plateau. Other galaxies with flat bars have also been found to have similar bar-profiles after subtraction of the bulge and disk. However, generally these bar profiles do not reach a plateau, but turn over and start to decrease immediately (e.g. IC 357).

We do not find a clear-cut correlation between bar profile type and Hubble type, in disagreement with Elmegreen et al. (1996). For the 24 most strongly-barred galaxies we can fairly unambiguously classify the bars as being either flat or exponential. Within this subset, we find that 13 galaxies are of type Sa–Sb, and of these 8 (62%) have flat bars and 5 (38%) exponential bars. For the 11 galaxies of types Sbc–Sd, 5 (45%) have flat bars and 6 (55%) exponential bars. Thus no correlation is found between bar type and Hubble type, although we are clearly suffering from small number statistics. There is a hint of a correlation between bar type and B/D ratio in the sense predicted by Elmegreen et al. (1996), since the mean B/D for galaxies with flat bars is 0.39 ± 0.16 , c.f. 0.21 ± 0.14 for galaxies with exponential bars.

The other measure of the bar major axis profiles comes from the radial dependence of EA, shown for a representative galaxy in Figure 15. Normalised to the underlying disk and bulge in this way, the bar profiles generally show a smooth increase in the central regions, where the dominance of the bulge is decreasing with radius, and a decrease at large radii where the fall-off is clearly much steeper than the exponential profile of the disk. None of the profiles show an extended plateau in these EA plots as might be expected, for example, were the bar to represent simply an enhancement of the underlying disk density at a given radius. Thus it appears that bars, whether of the flat or LD forms, are separate entities from the bulge and disk, and with light distributions which do not relate in any simple fashion to these other components.

Figure 16 shows bar short-axis profiles for some of the more strongly-barred galaxies in the sample. These were made by collapsing all of the flux along the long axis of the bar from the centre out to one end, thus giving an intensity-weighted mean cross-section of the bar. These K-band cross

sections are generally smooth but significantly asymmetric, in marked distinction to the early-type galaxy bars investigated by Ohta et al. (1990), who found bar cross sections to be highly symmetric. The sense of asymmetry for our bars is generally that the leading edge has a steeper profile than the trailing edge, where these terms are defined assuming that the bars rotate in the same sense as the spiral arms, and that the arms are trailing. Figure 16 shows bar cross-sections for the galaxies IC 1764, IC 357 (typical cases with steeper leading edges), IC 568 (with a steeper trailing edge) and NGC 2529 (approximately symmetric).

We find a very wide range in axial ratios for the bars in our sample, ranging from $(b/a) = 0.094$ to 0.53, where the dimensions used are FWHM values from the bar (bulge and disk subtracted) profiles described above, as shown in Figures 14 and 16. This is a much more extreme range than found in previous studies with, for example, Baumgart & Peterson (1986) finding only values in the range 0.35–0.55. The main discrepancy seems to lie in the very elongated bars we find, with major axis FWHM, in two cases, an order of magnitude larger than minor axis FWHM ($b/a = 0.094$ for NGC 2529, 0.096 for UGC 6332). In a few cases the minor axis FWHM is barely larger than the seeing scale, which may lead to the minor axis values in Table 3 being overestimated somewhat. Table 3 only shows minor axis and major axis profiles for 24 galaxies. These are the only galaxies for which we can get reliable values for these parameters. In the other barred galaxies the bar is either similar in size to the seeing or easily confused with the bulge. However, EA has still been calculated for all bars, because this is unaffected by seeing effects as explained earlier.

Figure 17 shows the bar lengths in kpc plotted against the bulge half-light radii. It has been suggested, both on the basis of numerical models (Sellwood 1981) and optical imaging (Athanassoula & Martinet 1980, Baumgart & Peterson 1986), that these quantities may be related, with longer bars being found in galaxies with larger bulges. However, this correlation is not borne out by the present data. We also find no correlation between bar length and B/D ratio.

7 CONCLUSIONS

We now summarise the main results from this study of spiral galaxy bulges, disks and bars, concentrating on those which seem discrepant from previously published results.

We find that bulge profiles are best fitted by $R^{1/2}$ or exponential profiles, in agreement with de Jong (1996b). However, we find no correlation between the index of the best-fit bulge profile and Hubble type, B/D ratio or bulge luminosity. B/D ratio also appears to correlate only weakly with Hubble type, and we concur with de Jong (1996b) in concluding that some other parameter must be the main determinant of morphological type.

Approximately 1/3 of our sample show significant central reddening in their J–K colours. This central reddening can be extended, which we take as evidence for a central starburst nucleus, or it can be unresolved, which we interpret as a dust-embedded AGN. The strongest examples of these phenomena are IC 568, which appears to have a strong nuclear starburst, and UGC 3707, which probably harbours a luminous Seyfert nucleus.

Bars are found in 40 galaxies, out of a total sample size of 45. Of the barred galaxies, 9 were classified as unbarred in the RC3 on the basis of their optical morphologies. Since our sample selection is unbiased with respect to bar strength, we believe this indicates that most, and quite possibly all bright spirals are barred at some level.

We determine bar strengths using a newly-defined, distance- and seeing-independent parameter called Equivalent Angle. This is preferred over the traditional bar-interbar method, because the latter can be strongly affected by seeing and other resolution effects. We find that bar strength does not correlate with disk K-band surface brightness, but that the strongest bars are found in a narrow, intermediate range of B/D.

We find two types of bar profiles, flat and exponential, in agreement with the finding of Elmegreen et al. (1996). However, we differ with Elmegreen et al. (1996) in finding no correlation between bar type and Hubble type. The K-band minor-axis bar profiles are significantly asymmetric, being generally steeper on the leading edge than on the trailing edge, assuming that the arms have a trailing geometry. Again this asymmetry is not predicted by any of the theoretical bar models, and was not found in the strongly barred galaxies investigated by Ohta et al. (1990). Finally, bar axial ratios were found to extend over a much large range of values than claimed from optical studies (Baumgart & Peterson 1986), with major axes up to ~ 10 times greater than minor axes.

8 ACKNOWLEDGEMENTS

We wish to thank Chris Collins and the referee for their useful comments in the preparation of this paper. The United Kingdom Infrared Telescope is operated by the Joint Astronomy Centre on behalf of the U.K. Particle Physics and Astronomy Research Council. This research has made use of the NASA/IPAC Extragalactic Database (NED) which is operated by the Jet Propulsion Laboratory, California Institute of Technology, under contract with the National Aeronautics and Space Administration.

REFERENCES

Aaronson M., Huchra J., Mould J., 1979, *ApJ*, 229, 1
 Andredakis Y.C., Sanders R.H., 1994, *MNRAS*, 267, 283
 Andredakis Y.C., Peletier R.F., Balcells M., 1995, *MNRAS*, 275, 874
 Athanassoula E., Martinet L., 1980, *A&A*, 87, L10
 Baumgart C.W., Peterson C.J., 1986, *PASP*, 98, 56
 Balzano V.A., Weedman D.W., 1981, *ApJ*, 243, 756
 Bertin G., Lin C.C., Lowe S.A., Thurstans R.P., 1989a, *ApJ*, 338, 78
 Bertin G., Lin C.C., Lowe S.A., Thurstans R.P., 1989b, *ApJ*, 338, 104
 Capaccioli M., Caon, N., 1992, in Longo G., Capaccioli M., Busarello G., eds., *Morphological and physical classification of galaxies*, Kluwer, Dordrecht, p.99
 Combes F., Debbash F., Friedli D., Pfenniger D., 1990, *A&A*, 233, 82
 Courteau S., de Jong R.S., Broeils A.H., 1996, *ApJ*, 457, L73
 de Jong R.S., 1996a, *A&AS*, 118, 557
 de Jong R.S., 1996b, *A&A*, 313, 45
 de Vaucouleurs G., 1953, *MNRAS*, 113, 134
 de Vaucouleurs G., 1963, *ApJS*, 8, 31
 de Vaucouleurs G., de Vaucouleurs A., Corwin H.G. Jr., Buta R.J., Paturel G., Fouqué P., 1991, *The Third Reference Catalog of Bright Galaxies*, Univ. Texas Press, Austin [RC3]
 Elmegreen B.G., Elmegreen D.M., 1985, *ApJ* 288, 438
 Elmegreen B.G., Elmegreen D.M., Chromei F.R., Hasselbacher D.A., Bissell B.A., 1996, *AJ*, 111, 2233
 Elmegreen D.M., Elmegreen B.G., 1984, *ApJS*, 54, 127
 Frankston M., Schild R., 1976, *AJ*, 81, 500
 Freeman K.C., 1966, *MNRAS*, 133, 47
 Freeman K.C., 1970, *ApJ*, 160, 811
 Friedli D., Benz W., 1993, *A&A*, 268, 65
 Gerola A., Seiden P., 1978, *ApJ*, 223, 129
 Glass I.S., Moorwood A.F.M., 1985, *MNRAS*, 214, 429
 Hohl F., 1971, *ApJ*, 168, 343
 Huang J.H., Gu Q.S., Su H.J., Hawarden T.G., Liao X.H., Wu G.X., 1996, *A&A*, 313, 13
 James P.A., 1994, *MNRAS*, 269, 176
 Kent S.M., Dame T., Fazio G., 1991, *ApJ*, 378, 131
 Kormendy J., Norman C.A., 1979, *ApJ*, 233, 539
 Lin C.C., Shu F., 1964, *ApJ*, 140, 646
 Lin C.C., Shu F., 1966, *Proc. Nat. Acad. Sci.*, 55, 229
 Miller R.H., Smith B.F., 1979, *ApJ*, 227, 785
 Ohta K., Hamabe M., Wakamatsu K.-I., 1990, *ApJ*, 357, 71
 Ostriker J.P., Peebles P.J.E., 1973, *ApJ*, 186, 467
 Pfenniger D., Norman C., 1990, *ApJ*, 363, 391
 Rix H.-W., Rieke M.J., 1993, *ApJ*, 418, 123
 Rix H.-W., Zaritsky D., 1995, *ApJ*, 447, 82
 Roberts W.W., Huntley J.M., van Albada G.D., 1979, *ApJ*, 233, 67
 Seigar M.S., James P.A., 1998, *MNRAS*, submitted (Paper II)
 Sellwood J.A., 1981, *A&A*, 99, 362
 Tully R.B., Fisher J.R., 1977, *A&A*, 54, 661
 Young C.K., Currie M.J., 1994, *MNRAS*, 268, L11

Table 1. The effect of seeing on extracted bulge and disk properties of simulated galaxies. Tabulated are model input and fitted output values.

Model	Bulge SB (counts)	Bulge radius (arcsec)	Bulge index	Disk CSB (counts)	Disk scale length (arcsec)
a	25000/24865	4.46/4.52	0.5/0.494	100/102	8.58/8.69
b	25000/26670	1.49/1.37	0.5/0.567	100/105	8.58/9.67

Table 2. Bulge and nuclear properties of the 45 spiral galaxies. The following data are included: Column 1, galaxy name; column 2, galaxy classification from RC3; column 3, galaxy redshift from NED; column 4, best-fit bulge index; column 5 bulge apparent magnitude at K; column 6 bulge half-light radius; and column 7, change in (J-K) colour within the central 5 arcsec in radius, which defines a central region large enough to be unaffected by variations in seeing.

Galaxy name	Hubble type (RC3)	Redshift (km s ⁻¹)	Bulge index	Bulge app. mag.	Bulge effective radius (arcsec)	Nuclear $\Delta(J - K)$
ESO 555-G013	Sa	2753	—	—	—	0.1
IC 357	SBab	6261	0.50	11.18	2.17	0.25
IC 568	SBb	8720	0.74	12.40	1.74	1.30
IC 742	SBab	6425	0.50	12.20	2.09	0.35
IC 1196	Sa	4885	0.49	12.54	2.00	0.30
IC 1764	SBb	5029	0.44	12.14	1.83	0.1
IC 1809	SBab	5578	0.37	11.37	1.74	0.3
IC 2363	SBbc	7616	0.53	12.45	1.89	0.2
IC 3692	SBa	6542	0.37	11.85	1.63	0.1
NGC 1219	SAbc	6101	0.49	11.84	2.09	0.2
NGC 2416	Sed	5101	0.50	10.96	1.72	0.1
NGC 2503	SABbc	5506	0.50	13.32	1.32	0.3
NGC 2529	SBd	5029	0.50	13.19	1.97	0.25
NGC 2628	SAbc	3622	0.60	12.45	1.72	0.15
NGC 3512	SABC	1376	0.60	11.99	1.80	—
NGC 5478	SABbc	7539	0.90	11.83	2.80	0.15
NGC 5737	SBb	9517	0.39	11.81	1.63	0.2
NGC 6347	SBb	6144	0.50	13.52	2.06	0.1
NGC 6379	Sed	5973	0.94	12.28	3.26	0.15
NGC 6574	SABbc	2282	0.50	13.23	1.83	0.20
UGC 850	SAbc	17283	0.48	13.76	1.34	0.25
UGC 1478	SBC	4846	0.90	12.47	5.41	0.0
UGC 1546	SABC	2374	1.00	13.73	4.32	0.2
UGC 2303	SABb	6404	0.50	12.21	1.26	0.05
UGC 2585	SBb	6847	0.60	11.98	1.54	0.0
UGC 2705	SBcd	6858	0.40	12.76	3.15	0.05
UGC 2862	SABA	6644	0.54	10.53	2.77	0.05
UGC 3053	Sed	2407	0.63	9.73	1.32	—
UGC 3091	SABd	5559	0.34	14.12	3.58	0.05
UGC 3171	SBcd	4553	0.58	12.04	1.52	0.1
UGC 3233	Sed	4662	0.95	13.63	4.92	0.05
UGC 3296	Sab	4266	0.54	12.82	1.72	0.00
UGC 3578	SBab	4531	0.43	11.44	1.57	0.15
UGC 3707	Sab	5967	0.58	12.13	1.83	0.85
UGC 3806	SBcd	5484	0.45	14.11	1.40	0.35
UGC 3839	SBb	5267	0.49	12.65	2.00	0.30
UGC 3900	SBb	8535	0.47	12.84	2.06	0.0
UGC 3936	SBbc	4725	0.57	11.89	1.72	0.15
UGC 4643	SAbc	7699	0.57	12.69	1.86	0.00
UGC 5434	SABb	5580	0.43	13.42	2.15	0.00
UGC 6166	Sbc	10182	0.57	15.21	2.89	—
UGC 6332	SBa	6245	0.52	10.74	1.74	0.05
UGC 6958	SABbc	5931	0.97	12.49	2.43	0.05
UGC 8939	SABb	7459	0.46	12.12	2.20	0.15
UGC 11524	SAC	5257	0.87	12.28	4.66	0.15

Table 3. Disk and bar properties of the 45 spiral galaxies. The following data are presented: column 1, galaxy name; column 2, disk central surface brightness; column 3, disk scale length; column 4, disk apparent magnitude; column 5, bulge-to-disk ratio; column 6, bar strength; column 7, bar FWHM along major axis; column 8, bar FWHM along minor axis; and column 9, bar type.

Galaxy Name	Disk CSB (K mag)	Disk scale length (arcsec)	Disk app. mag.	B/D	Bar EA	Bar long axis (arcsec)	Bar short axis (arcsec)	Bar type
ESO 555 -G 013	18.20	9.7	10.69	—	—	—	—	—
IC 357	16.47	8.6	10.02	0.34	23	13.3	2.2	Flat
IC 568	18.23	10.8	11.58	0.47	80	20.8	3.0	Flat
IC 742	18.88	24.7	10.46	0.2	18	15.7	2.6	Flat
IC 1196	16.12	4.0	11.73	0.49	4	—	—	—
IC 1764	18.12	12.0	10.78	0.29	27	11.2	3.6	Flat
IC 1809	16.90	6.4	11.27	0.91	16	5.9	3.1	Exponential
IC 2363	17.62	8.1	11.22	0.32	36	13.1	2.1	Exponential
IC 3692	19.48	7.5	10.92	0.42	42	8.3	1.25	Exponential
NGC 1219	17.31	11.4	10.07	0.20	5	—	—	—
NGC 2416	17.50	12.3	10.51	0.66	9	—	—	—
NGC 2503	17.71	8.6	11.06	0.13	9	13.9	4.1	Flat
NGC 2529	17.18	7.1	11.30	0.18	13	12.7	1.2	Exponential
NGC 2628	17.34	11.4	10.10	0.12	12	6.6	1.7	Flat
NGC 3512	16.56	11.4	9.40	0.09	12	—	—	—
NGC 5478	17.75	12.1	10.76	0.37	7	—	—	—
NGC 5737	17.31	11.5	10.59	0.33	63	10.1	2.3	Exponential
NGC 6347	17.08	9.8	10.74	0.08	15	—	—	—
NGC 6379	17.83	14.3	10.26	0.16	7	—	—	—
NGC 6574	17.43	8.1	11.17	0.15	8	—	—	—
UGC 850	18.36	8.6	11.98	0.19	6	—	—	—
UGC 1478	18.52	11.9	11.33	0.35	20	7.0	2.0	Exponential
UGC 1546	18.52	8.5	11.89	0.18	—	—	—	—
UGC 2303	17.48	7.6	11.07	0.35	34	6.1	1.0	Exponential
UGC 2585	17.48	10.0	10.82	0.34	17	13.2	2.0	Flat
UGC 2705	19.15	11.4	12.02	0.50	22	6.2	1.25	Flat
UGC 2862	19.23	25.7	11.02	1.56	8	—	—	—
UGC 3053	16.35	12.1	9.27	0.65	—	—	—	—
UGC 3091	18.91	9.7	11.84	0.15	—	—	—	—
UGC 3171	17.57	8.9	11.06	0.40	8	4.8	1.1	Flat
UGC 3233	19.45	11.4	12.43	0.33	10	—	—	—
UGC 3296	16.33	6.3	10.68	0.14	6	—	—	—
UGC 3578	16.02	7.8	10.31	0.35	39	15.5	3.0	Flat
UGC 3707	18.02	18.0	11.03	0.36	62	—	—	—
UGC 3806	18.65	12.9	11.31	0.08	12	8.8	1.8	Flat
UGC 3839	18.01	10.0	11.15	0.25	20	14.0	2.2	Flat
UGC 3900	17.93	8.7	11.49	0.29	21	5.7	1.1	Exponential
UGC 3936	16.79	8.6	10.34	0.24	16	8.4	1.6	Exponential
UGC 4643	18.33	9.7	11.65	0.38	6	—	—	—
UGC 5434	18.16	15.7	10.61	0.08	5	—	—	—
UGC 6166	17.13	7.8	13.57	0.22	—	—	—	—
UGC 6332	17.65	15.1	9.98	0.49	23	12.5	1.2	Flat
UGC 6958	18.00	17.5	10.20	0.12	22	5.9	1.65	Exponential
UGC 8939	18.65	14.2	11.09	0.39	20	7.8	1.4	Exponential
UGC 11524	18.39	15.7	10.66	0.22	5	—	—	—

Figure 1. Examples of the K-band galaxy light profiles produced by the ellipse-fitting process. Lines show the best fits obtained using the sum (dashed line) of an exponential disk (dotted line), and a generalised de Vaucouleurs profile (dash-dotted line) for the bulge.

Figure 2. Best fitting bulge index in the generalised de Vaucouleurs profile, plotted against Hubble type.

Figure 3. Best fitting bulge index in the generalised de Vaucouleurs profile, plotted against integrated K-band bulge absolute magnitude.

Figure 4. Central J-K colour profiles in selected galaxies.

Figure 5. Disk K-band central surface brightness plotted against disk absolute K magnitude.

Figure 6. Disk K-band central surface brightness plotted against Hubble type.

Figure 7. Galaxy K-band bulge-to-disk ratio plotted against Hubble type.

Figure 8. Disk exponential scale length plotted against bulge half-light radius.

Figure 9. Disk K-band central surface brightness plotted against disk exponential scale length.

Figure 10. Diagrammatic representation of equivalent angle.

Figure 11. The ranges of bar strengths, measured in averaged equivalent angle (see text for definition). The black areas represent the bar strengths of those galaxies with near neighbours.

Figure 12. Bar strength plotted against disk K-band central surface brightness.

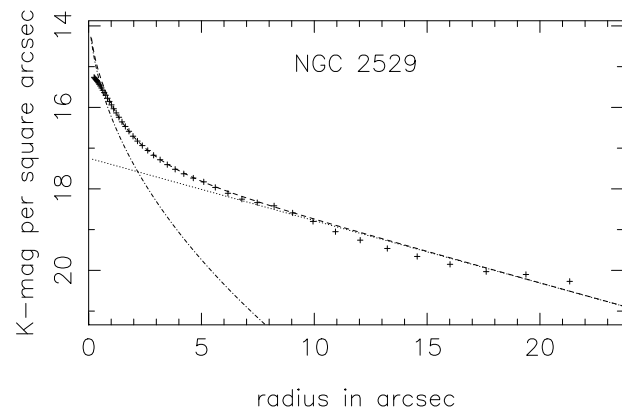
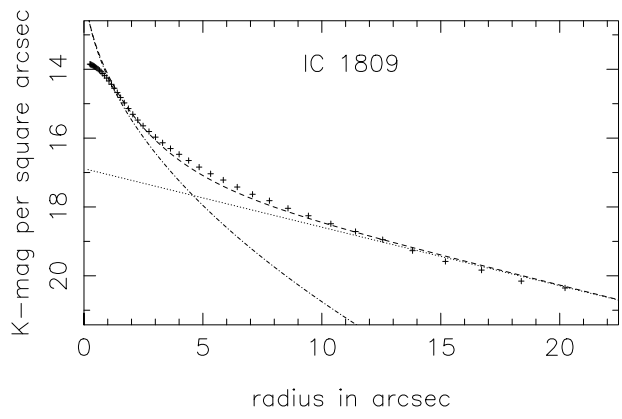
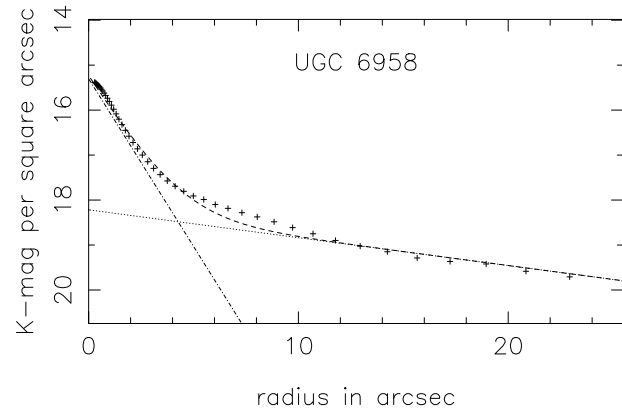
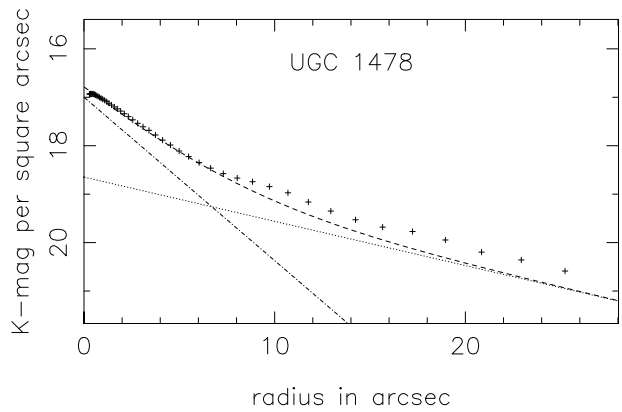
Figure 13. Bar strength plotted against K-band bulge-to-disk ratio.

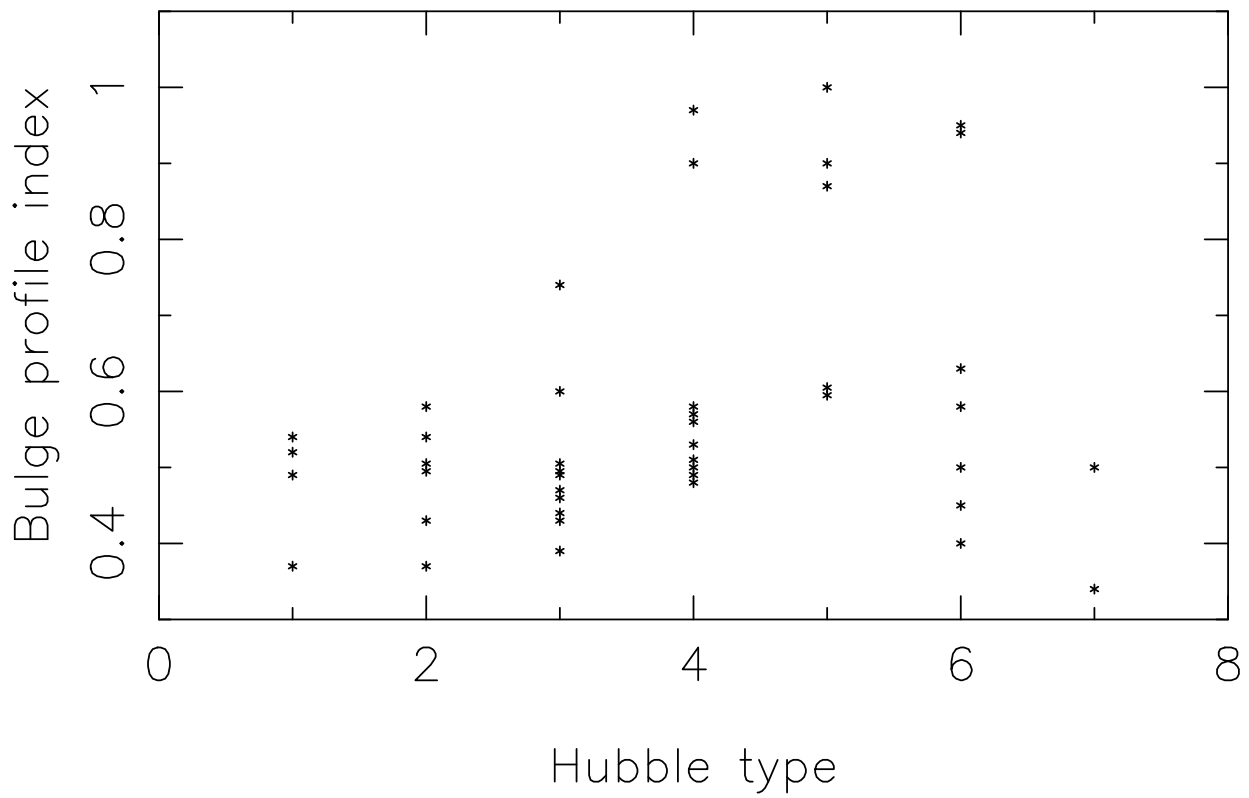
Figure 14. Bar profiles without disk- and bulge-subtraction (left column) and with disk- and bulge-subtraction for three representative galaxies.

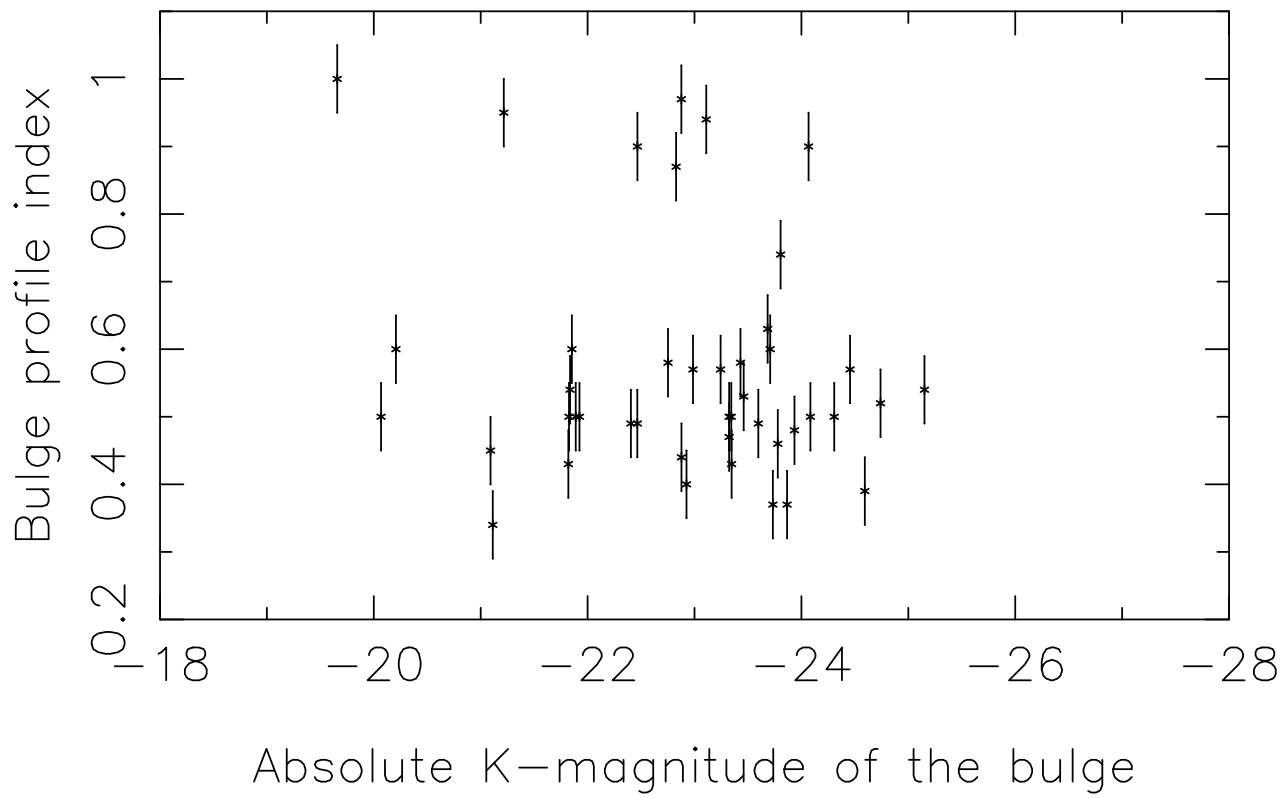
Figure 15. Bar strength in equivalent angle plotted against radius for IC 568.

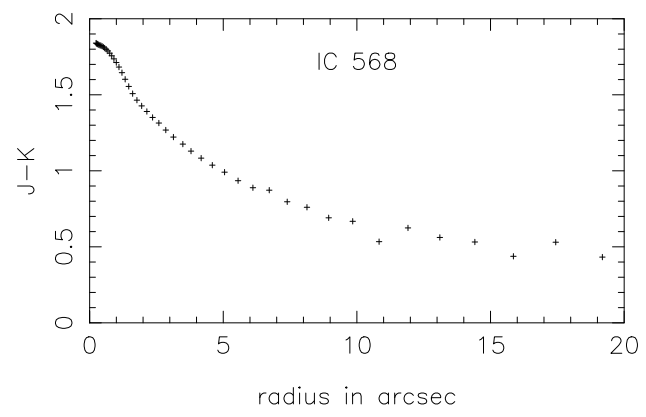
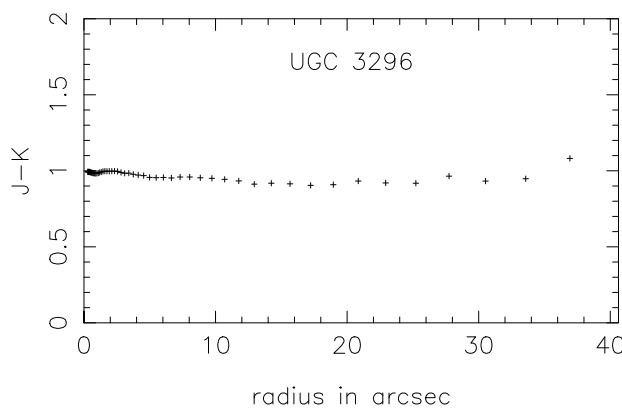
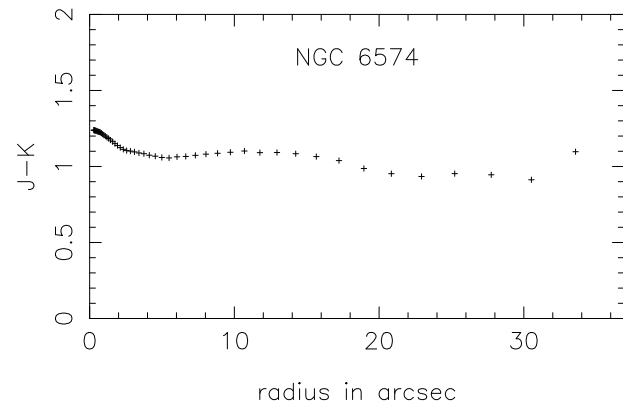
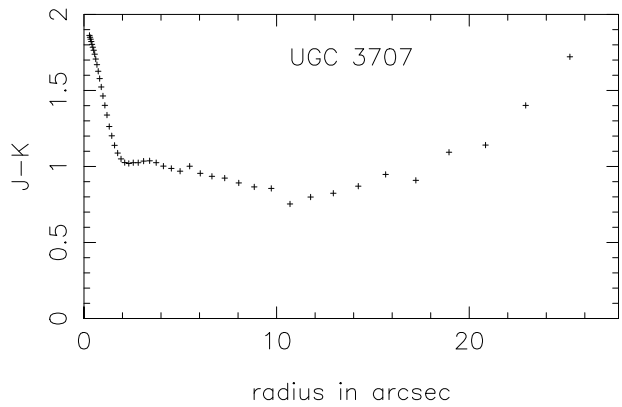
Figure 16. Four bar cross-sections with two typical cases (IC 1764 and IC 357) with steeper leading edges one case (IC 568) with a steeper trailing edge and one case (NGC 2529) approximately symmetric. The ‘leading’ edge is plotted on the right.

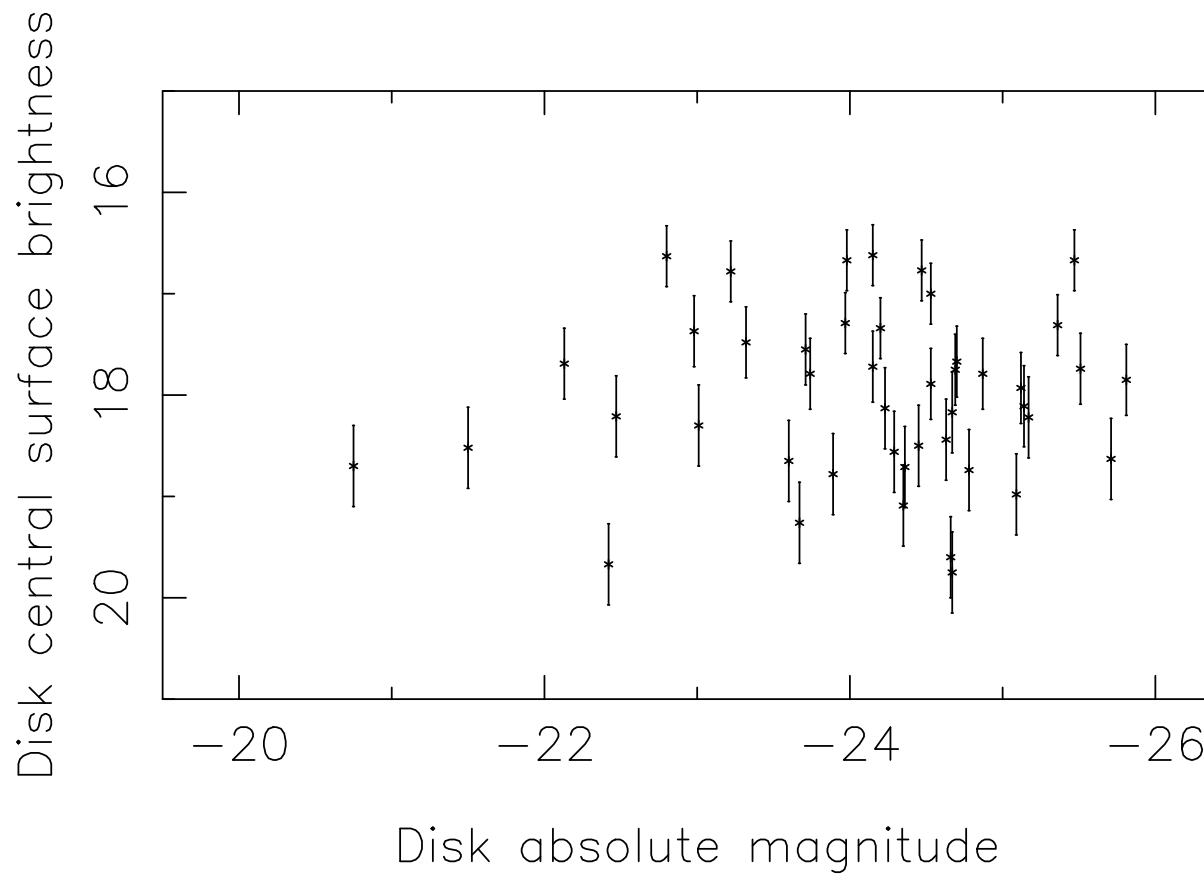
Figure 17. Bar length plotted against bulge half-light radius.

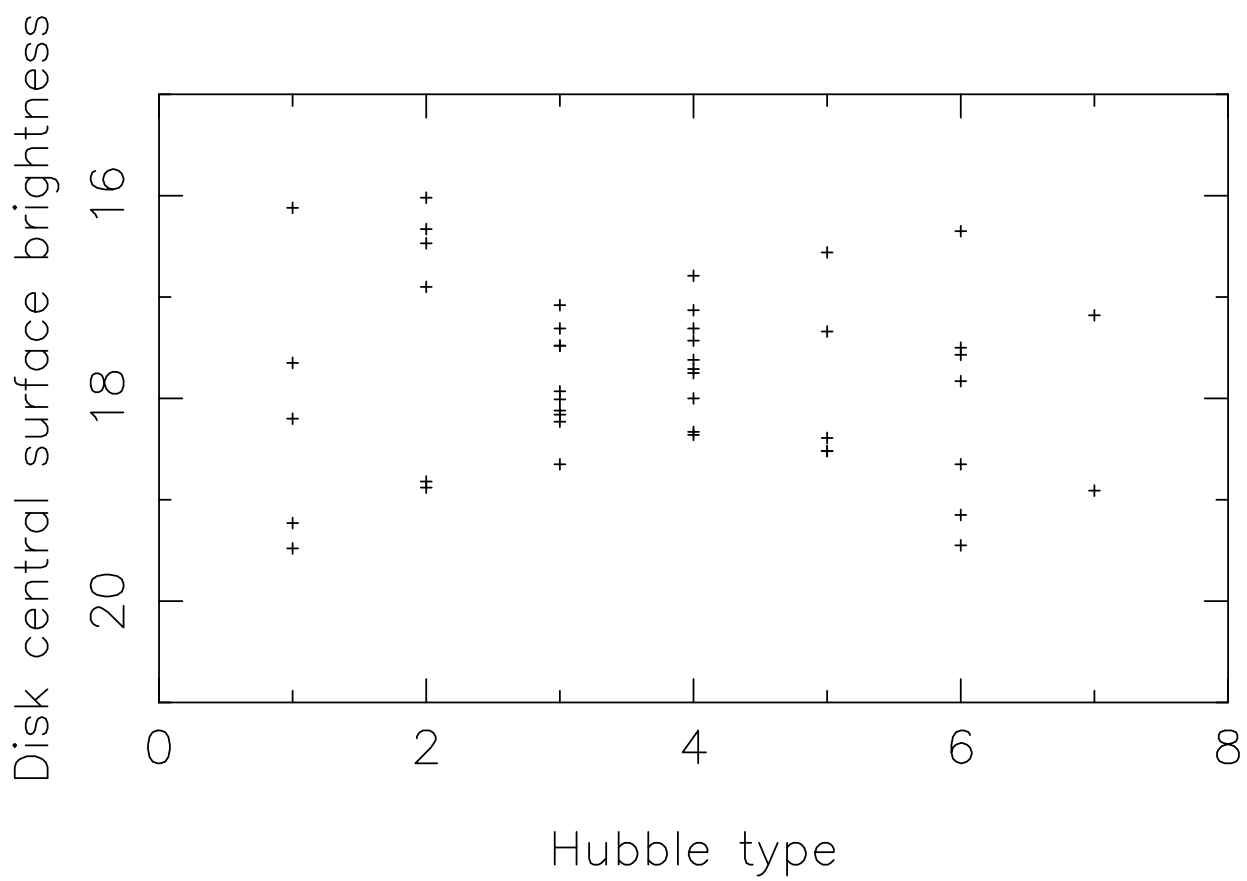


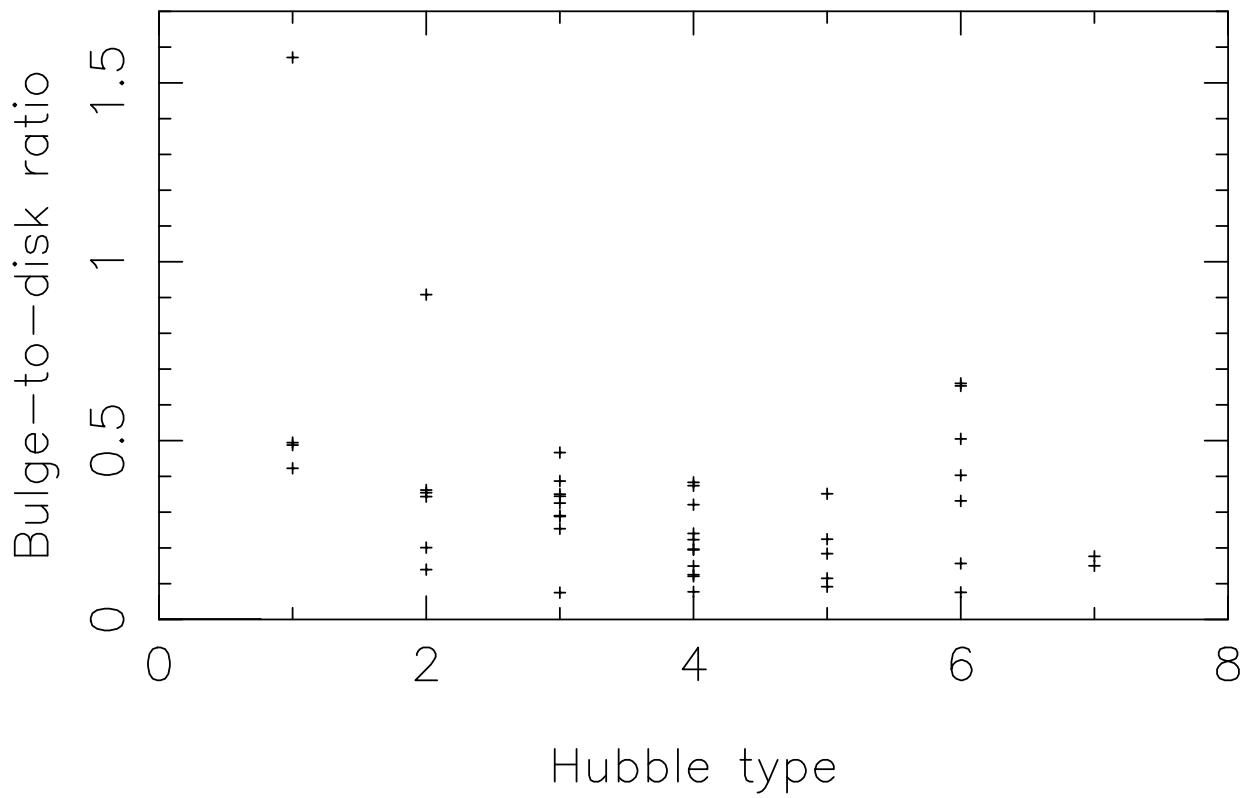


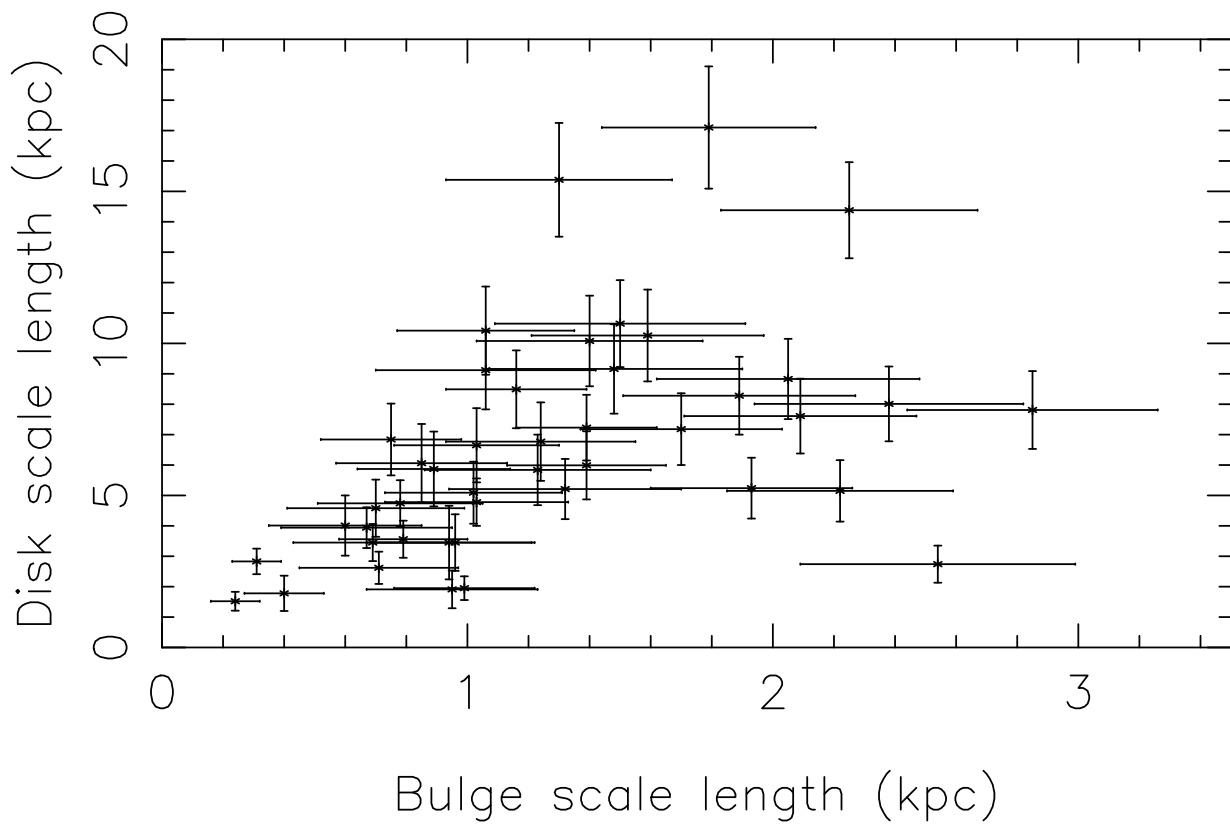


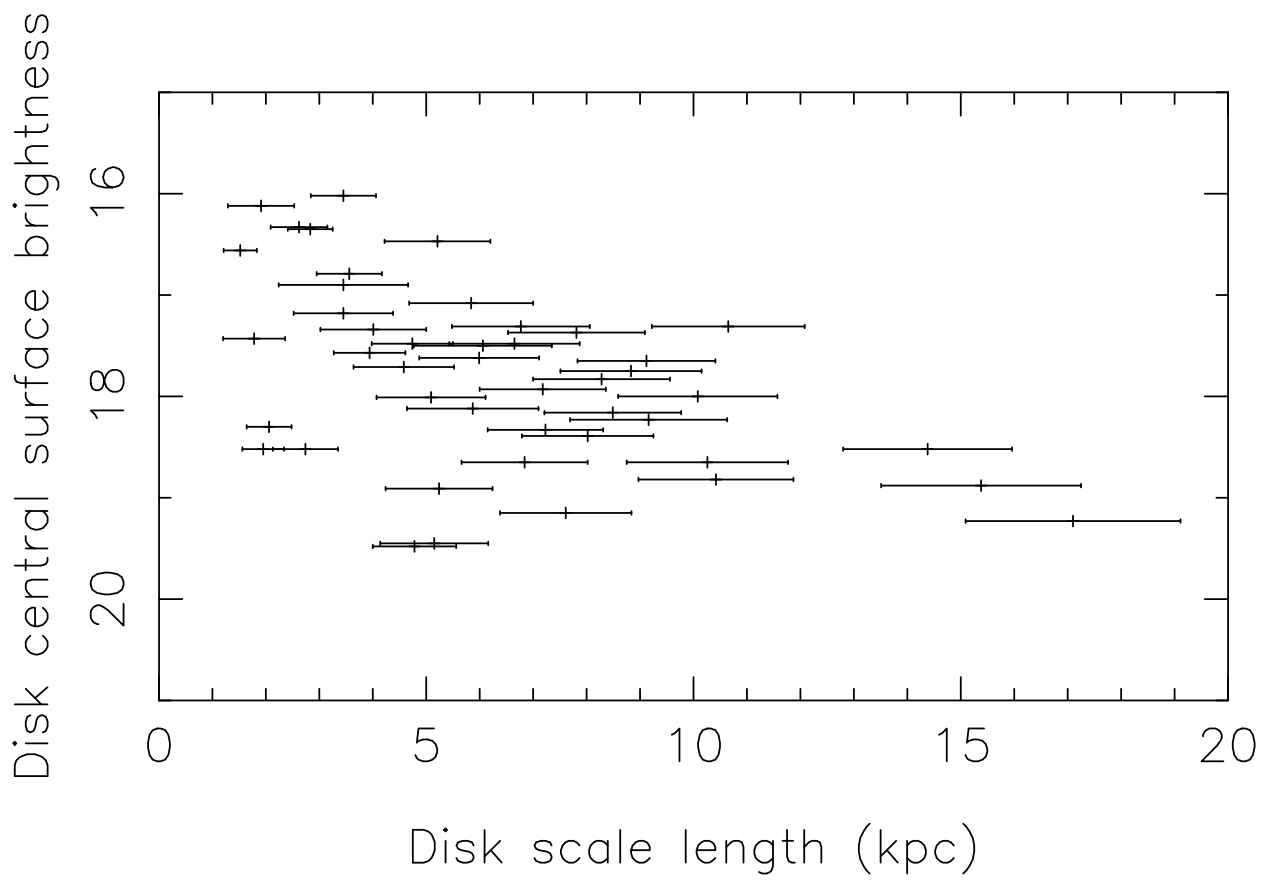


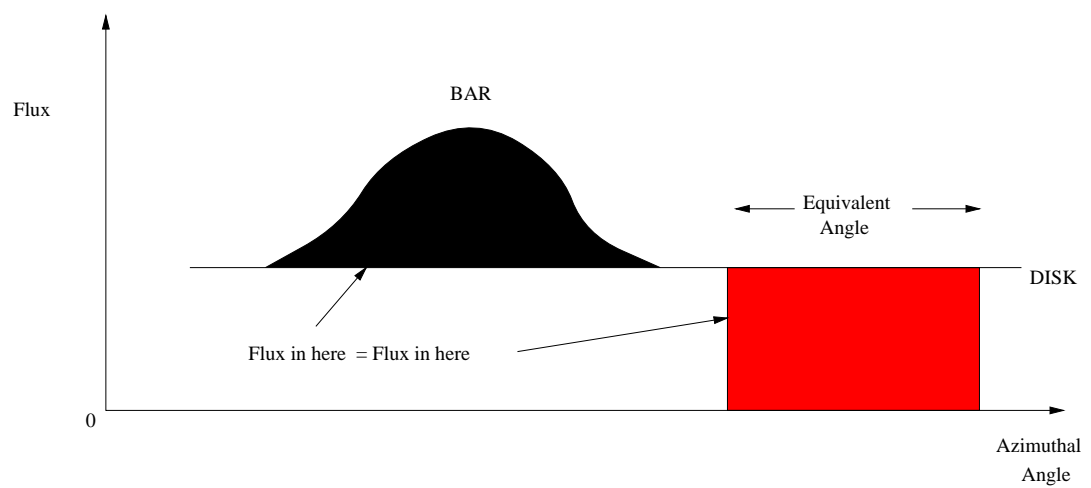


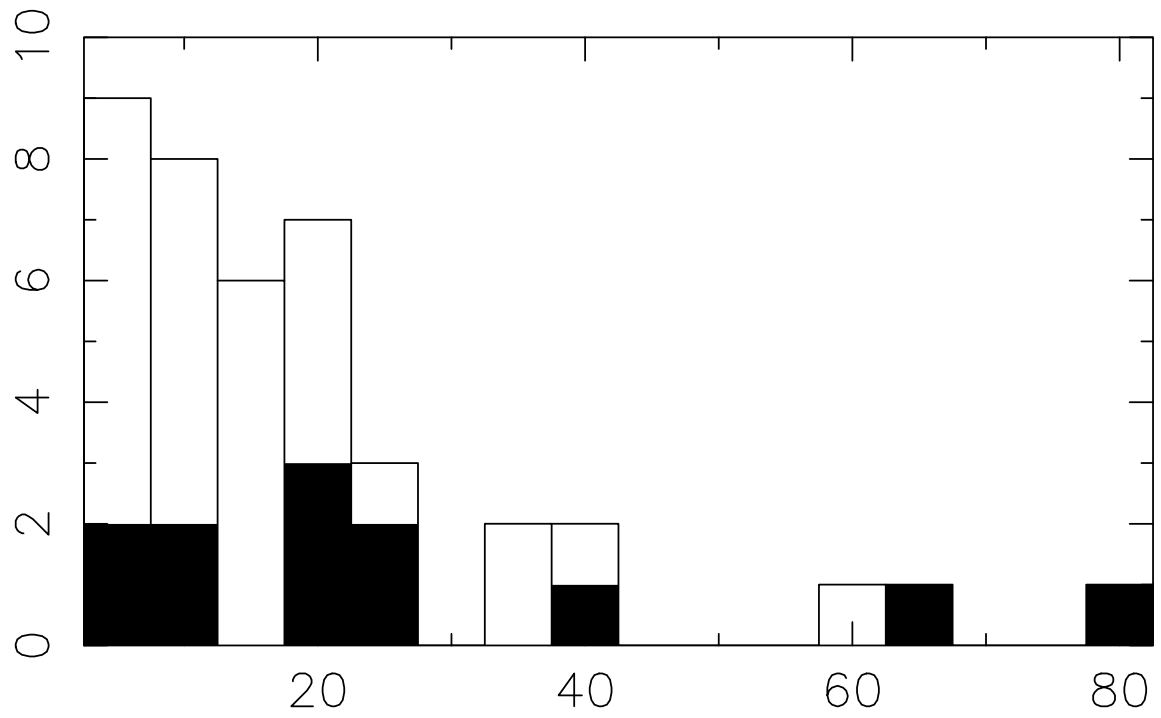












Bar strength in terms of overall EA

